

A Biomimetic Approach to Improve Convective Heat Transfer Using Fluid-Induced Vibrations from Self-Excited Flaps

Sahand Najafpour¹ and Majid Bahrami²

Laboratory for Alternative Energy Conversion (LAEC),
School of Mechatronic Systems Engineering, Simon Fraser University, Surrey, BC, Canada
Sahand_najafpour@sfu.ca; Majid_bahrami_2@sfu.ca

ABSTRACT - Bio-inspired flexible plates have shown promising results as a passive method to enhance convective heat transfer and mixing in flow. Flap fluttering is a self-excited phenomenon caused by the fluid-structure-interaction between the main flow and the flap. Among all the parameters, the direction of the flap relative to the incoming flow appears to be the key factor in determining the transition into the flapping mode. In this study, flaps made of a 50-micron thick polyester sheet were cut into rectangular shapes and placed at the centerline of the channels of a shrouded straight fin heatsink. Both hanging and vertical positions of the flap in the axial flow were investigated using a custom-built testbed in our lab. We measured the convective heat transfer rates and pressure drop in the heatsink for both arrangements. We observed that: i) the rectangular cantilevered flap is more unstable in the hanging flap configuration compared to the vertically installed flap, i.e., the transition to the fluttering mode occurs at a lower airflow velocity; ii) the critical flow velocity – the velocity at which the flap becomes unstable – is lower for the flap aspect ratio of 0.5. We attribute this behavior to the longer viscous boundary layer around the vertical case, which stabilizes the flap; iii) from a thermal performance point of view, the hanging configuration outperforms the vertical one with the same flap dimensions; iv) at a Reynolds number of 8,940, large amplitude vibrations and coherent fluttering in a hanging configuration render a superior thermal performance of 39 percent improvement in the Nusselt number compared to when bare channels are measured. On the contrary, at higher flowrates, the difference falls in the range of measurement uncertainty; and v) as for the pressure drop, unlike the hanging configuration, the vertical flap creates a higher pressure drop as it tends to block half the channel at the end of the trailing edge stroke. Furthermore, the presence of the flap holder adds to the pressure drop increase, which is eliminated in the hanging position and therefore, flaps could be connected to the shroud directly.

Keywords: Flap fluttering, Hanging flap configuration, Fluid-structure-interaction, Convective heat transfer, Critical flow velocity

1. Introduction

Forced convection heat transfer is used predominantly for electronic cooling and heat exchangers with moderate to relatively high-density heat fluxes [1]. However, as the thermal boundary layer develops, the heat transfer rate degrades and plateaus to a constant value. The everchanging technological advancement requires more compact components with higher heat generation rates in the electronic industry, solar power systems, power plants, etc. This leads to a heat flux spike, which demands more efficient heat dissipation and generally better thermal management [2]. One approach to improve the heat transfer rate is to interrupt the boundary layer. Also, the turbulent flow is more efficient in terms of the heat exchange between the fluid and the surface. As a result, numerous studies have been conducted on the use of vortex generators as turbulators confirming their superiority to mix the flow and enhance the heat transfer over other strategies [3], [4]. Among all the vortex generators, flexible plates known as flaps or flaps have shown promising results. The flaps are placed along the flow and initiate vibration at a certain flow velocity called *critical flow velocity* and maintain their movement forward [5]. The critical flow velocity and the effect of spanwise clearance have been studied intensively in wind tunnels to find the underlying physical parameters governing the transition to the flapping mode [6]–[9]. This bio-inspired method has drawn attention recently as the tip vortices generated due to the self-sustained fluttering of the flexible plate can enhance the heat transfer coefficient at a relatively low pressure drop cost. The behavior of the flaps is classified into three distinct modes: i) the stretched straight mode; ii) the flapping or fluttering mode; and iii) the deflected mode, see Fig. 1 [10], [11]. Generally, the flap is initially stationary at low flowrates as the destabilizing perturbations are not sufficient to trigger flapping. In this regime, vortices with alternating signs are generated and advected by the main flow downstream, but they do not contribute

to heat transfer enhancement [12], [13]. The onset of fluttering that happens at the critical flow velocity depends on both the fluid characteristics and the physical properties of the flexible plate [14], [15].

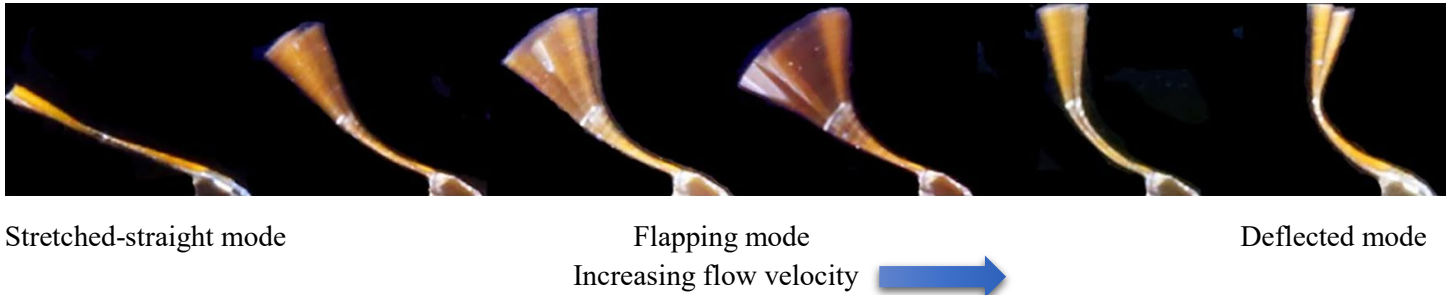


Fig. 1: Distinctive flap modes as airflow increases [10].

Once the transition to the flapping mode occurs, coherent large amplitude vibrations are observed. The pressure difference across the flap is the principal reason for deflections and the elastic restoring forces are responsible for sustaining the flapping [16]. By further increasing the flowrate, the transition to the deflected mode occurs as the elastic forces are not able to return the flap to its initial position. Zhong et al. [17] tested Kapton flaps installed vertically in a single channel and reported the positive effect of the split flag on the heat transfer due to the interaction between strips. A maximum thermal-hydraulic performance factor of 1.91 has been reported for the case with four strips. They also conducted an experimental study on an inverted flap, where the trailing edge was clamped instead of the leading edge [11]. Although, the transition to the flapping mode occurred at a lower airflow, the friction coefficient was augmented 6 to 8-fold, while achieving only an 80% increase in the Nusselt number. Furthermore, Li et al. [10] investigated hourglass-shaped agitators, different numbers and various pitches. They reported that an optimum distance between two consecutive flaps was 25 mm. Nonetheless, the pressure loss owing to the airflow blockage in the deflected mode eclipsed with an almost 200% increase in Nu number compared to the bare channel at Reynolds numbers higher than 5,000. In another experimental study, the advantage of using two pairs of rectangular flaps over stationary vortex generators was shown, where the convective heat transfer was enhanced by matching the heatsink’s preferred frequency mode and the agitator’s resonance frequency [18]. An overview of the experimental studies on flap fluttering as a convective heat transfer enhancement method is provided in Table 1. As highlighted in Table 1, the focus of these studies has been on either parallel or inclined flaps. The question arises as to whether or not other configurations, namely horizontal and hanging, would be more effective. In this paper, we focused on the hanging configuration for its potential practical applications.

Table 1: An overview of published studies incorporating a flap as a vortex generator.

| | Flap Orientation | Flap Shape | Notes |
|----------------------|-----------------------------|------------------|---|
| Alison et al. [19] | Parallel, Standard Vertical | Rectangle | 25% Enhancement in Nu number at 35% hydraulic loss |
| Herrault et al. [20] | Parallel, Standard Vertical | Rectangle | 60% Heat transfer augmentation |
| Li et al. [21] | Parallel, Standard Vertical | Airfoil-shaped | 15% Heat transfer enhancement at the same pumping power |
| Li et al. [10] | Inclined angle (35°) | Hourglass-shaped | 68% Improvement in thermal-hydraulic performance |
| Zheng et al. [18] | Inclined angle (45°) | Rectangle | 120% Heat transfer increase at the same pumping power |

To summarize, the standard flag outperforms the inverted one in terms of heat transfer enhancement and the pressure drop penalty. The shortcoming of the vertical in-line flag configuration is the higher critical flow velocity, which requires more fan power and leads to excess noise. There are myriad number of factors determining the transition to the flapping mode, including: the flap dimensions, the momentum of the flow, the density of the solid, the flexural modulus, etc. [22]. Nonetheless, the position of the flaps in the channel with respect to the incoming flow is paramount. Although, numerous studies focused on the vertical configuration with various inclination angles [23], [24], to the best of our knowledge, no study

has ever been carried out on the hanging configuration. In this paper, we report our experimental results, including the critical flow velocity and hydrothermal performance of a parallel plate-fin heatsink equipped with flaps and compare the results with the bare heatsink.

2. Methodology

2.1. Experimental setup

A custom-built testbed has been developed in our lab and is shown schematically in Fig. 2. The testbed is comprised of the following main components: a counter blower attached to an airflow chamber with an orifice plate in between for measuring the air flowrate, i.e., a 1,000 mm × 90 mm × 30 mm channel made of acrylic sheets equipped with a heating section. The test section was wrapped with insulation material to minimize the heat loss. The heating section included a four-channel plate-fin heatsink with a length, width, and height of 300 mm, 40 mm, and 30 mm, respectively, glued to a heating block. The heating block had the same area as the heatsink and the film heater (flexible polyamide, Omega) was attached to the bottom of the heating block. The heating block was covered all around with an insulation material to minimize the heat loss and to ensure that a uniform 1-D heat flow was directed at the heatsink. The contraction section and air straighter were installed at the inlet to minimize the upstream turbulence. The temperature of the heating block was measured using 9 T-type thermocouples (Omega) that were inserted vertically at three locations. The inlet and outlet air temperatures were measured using RTDs (PT100, Omega) for a higher accuracy. Two pressure taps were used before and after the heatsink to measure the pressure drop using a differential pressure transducer (267, Setra). More details on the suppliers, models, and the accuracy of sensors used in the testbed can be found in Table 2.

Table 2: A list of measuring devices and their corresponding accuracy.

| Measurement Devices and Sensor | Model | Accuracy |
|--|---------------------|----------|
| Omega T-type Thermocouple | | ±0.5 °C |
| Omega RTD | PR-13-2-100-1/8-6-E | ±0.15 °C |
| Setra Differential Pressure Transducer | 2671-001WB-11-G1ED | ±0.4% |
| Lamda Orifice Plate | FLC-AC | < ±0.5% |
| Omega Polyimide Heater | KHA-112/10-P | |

The flaps were made of a 50-micron thick polyester (PET) film with a flexural rigidity of 4.89 GPa (McMaster-Carr). They were cut in rectangular shapes (24 mm × 12 mm). Since there is no general equation for thermal entrance length in a turbulent regime, we used the following approximation for the thermal entrance length [25]:

$$\frac{x_{th}}{D_h} = 10 \quad (1)$$

where, x_{th} is the thermal entrance length, and D_h (m) is the hydraulic diameter of a single heatsink channel. Consequently, one flap per channel was installed 150 mm from the channel entrance. For the vertical configuration, flaps were connected to a 0.02-mm stainless steel foil, as the flap mast; the hanging configuration didn't require a post and the flaps were connected to the heatsink shroud directly. The schematic diagram and a photo of the testbed are shown in Fig. 2. The installed flaps are depicted in Fig. 3

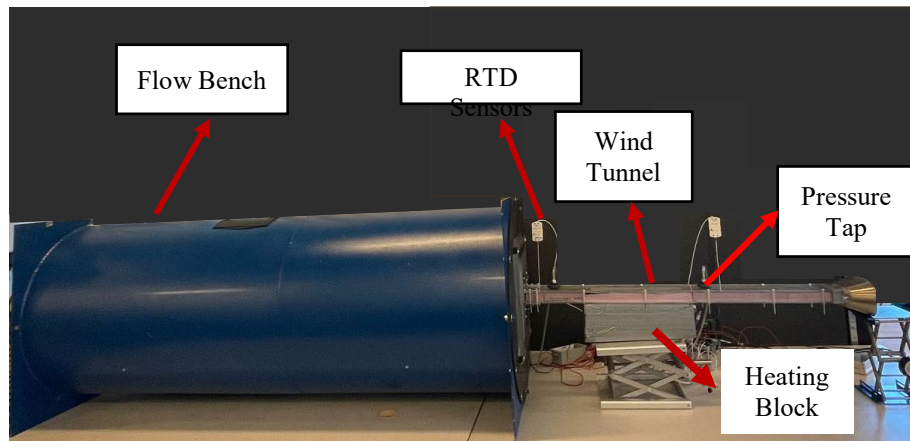
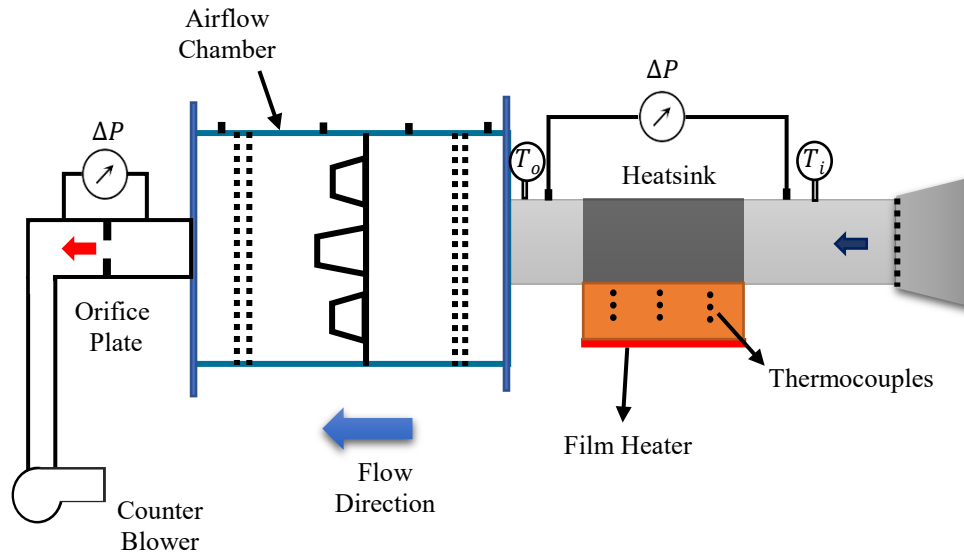


Fig. 2: A schematic diagram and photo of the testbed used to conduct the forced air convection experiment.

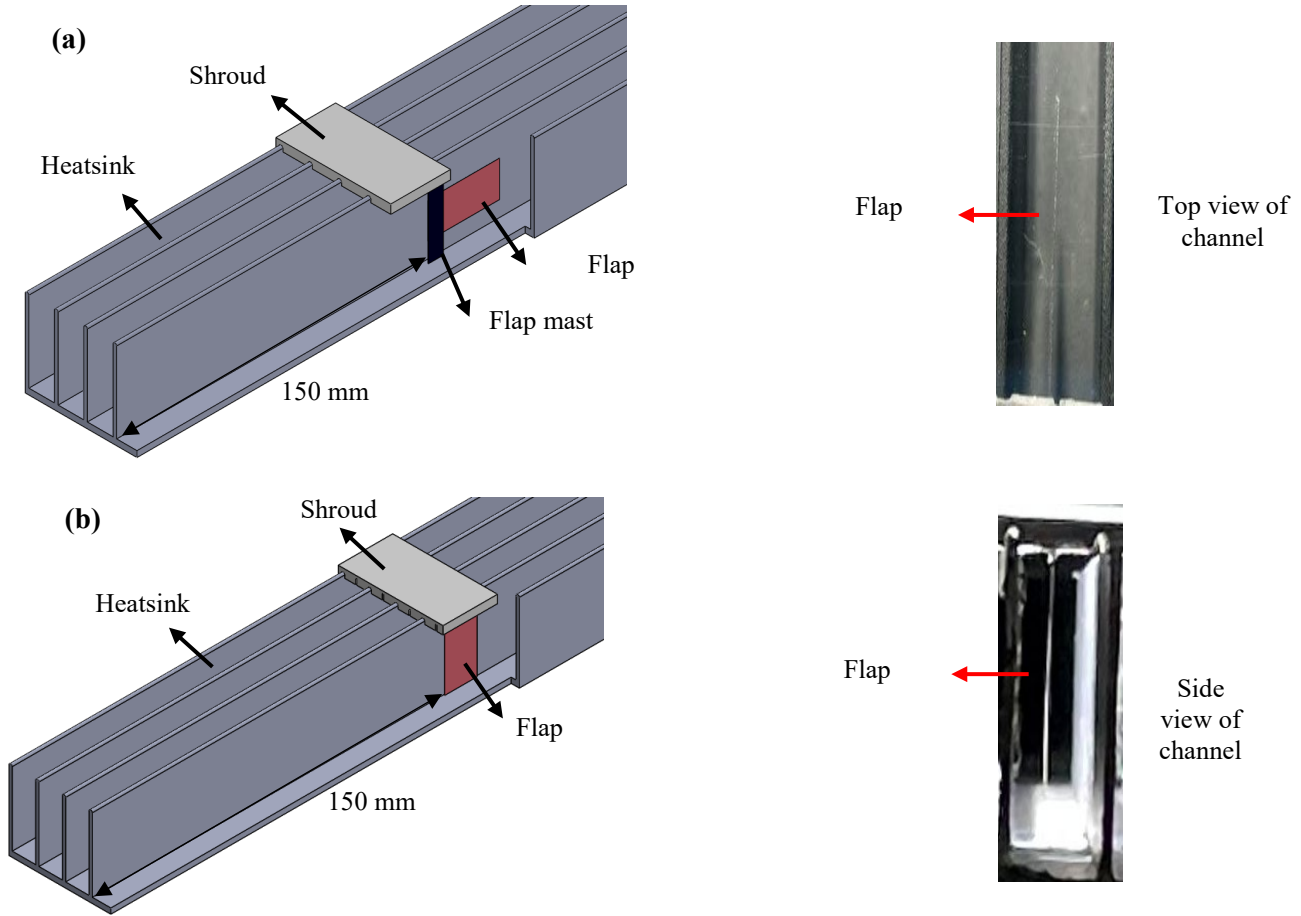


Fig. 3: The flaps placed in the channels of the heatsink in: (a) a vertical configuration with the top view photo; and (b) the hanging configuration with the side view photo.

2.2. Experimental Procedure And Data Analysis

Initially, the tests were conducted on the bare heatsink to establish a baseline for the results. The electrical power input was set and maintained to a predetermined value throughout the entire experiment. The fan was set to the suction mode to minimize the entrance disturbances. The airflow was modulated using a variable speed centrifugal fan. The airflow was increased step by step and the data were recorded once the steady-state condition was reached. The steady-state condition was assumed, when the temperature variation with respect to time was less than 0.1 °C per 5 minutes. Then, the tests were performed with agitators installed between the heatsink channel walls and connected to the shroud in two configurations: i) the vertical configuration; and ii) the hanging configuration.

In order to evaluate the performance of the heatsink, the following non-dimensional numbers are defined and used. The Reynolds number of the flow is defined as:

$$Re = \frac{\rho \dot{V} D_h}{4A_c \mu} \quad (2)$$

where, \dot{V} ($\frac{m^3}{s}$) is the airflow rate measured by the orifice plate, D_h (m) is the hydraulic diameter of a single heatsink channel as the characteristic length, A_c (m^2) is the cross-sectional area of one of the heatsink channels, ρ ($\frac{kg}{m^3}$) and ν ($\frac{m^2}{s}$) are the density and dynamic viscosity of the air at film temperature, respectively.

Since the pressure drop is a characteristic of the hydraulic performance, the friction factor is considered using Eq. (3):

$$f \equiv \frac{\Delta p D_h}{0.5 \rho U^2 L} \quad (3)$$

where, Δp (Pa) is the pressure drop across the test section, L (m) is the distance between the pressure taps, i.e., 0.4 m, and U ($\frac{m}{s}$) is the inlet average velocity, respectively.

To assess the thermal performance of the heatsink, the Nusselt number and j-factor are selected as shown in Eqs. (4) and (6), respectively.

$$Nu = \frac{h D_h}{k} \quad (4)$$

where, k ($\frac{W}{m.K}$) is the thermal conductivity of air and h ($\frac{W}{m^2.K}$) is the convective heat transfer coefficient derived from Eq. (5):

$$h = \frac{\dot{Q}}{A_t \Delta T_{LMTD}} \quad (5)$$

where, \dot{Q} (W) is the heat generated by the film heater transferred to the heatsink, A_t (m^2) is the total convective heat transfer area, and ΔT_{LMTD} (K) is the log mean temperature difference between the heatsink base temperature and the airflow temperature, respectively. As the uniform heat flux is applied to the bottom of the heatsink, the log mean temperature difference is used to calculate the heat transfer coefficient:

$$j \equiv \frac{Nu}{Re Pr^{\frac{1}{3}}} \quad (6)$$

where, Pr is the air Prandtl number defined as the ratio of momentum diffusivity to thermal diffusivity α ($\frac{m^2}{s}$):

$$Pr \equiv \frac{\nu}{\alpha} \quad (7)$$

Finally, the overall thermal-hydraulic performance is assessed using Eq. (8) in which the increase in heat transfer is divided by the increase in the fan/pumping power. In other words, the thermal-hydraulic performance factor determines the heat transfer enhancement at a constant pumping power compared to the baseline, where no flags were added.

$$\eta = \frac{\left(\frac{Nu}{Nu_0}\right)^{\frac{1}{3}}}{\left(\frac{f}{f_0}\right)^{\frac{1}{3}}} \quad (8)$$

The tests were repeated three times each, the results were repeatable with a maximum deviation of 6%; averaged values were used in this study.

Furthermore, an uncertainty analysis was carried out to account for both the bias and the random variation errors. The bias uncertainty analysis is calculated using a root-sum-square method following Ref. [26]:

$$\frac{\delta Y}{Y} = \sqrt{\sum_{i=1}^n \left(\frac{\delta X_i}{X_i}\right)^2} \quad (9)$$

where, Y is a function of (X_1, X_2, \dots, X_n) variables. The accuracy of the measurement devices used in our testbed are listed in Table 1. The overall uncertainty of our measurements is estimated to be less than 8%.

3. Results and Discussion

The experimental results for the friction coefficient and Nu number are presented in Figs. 3 and 4, respectively. The jump in both the friction factor and Nu number demarcates the transition to the flapping mode. The hanging flap jumped to

the flapping mode at a 19% lower critical flow velocity in comparison with the vertical flap. Since the source of excitation in both configurations was movement-induced [27], we believe that the lower airflow velocity associated with the hanging flap is due to the shorter viscous boundary layer around it. The viscous boundary layer resists the perturbations, which in turn stabilizes the flap.

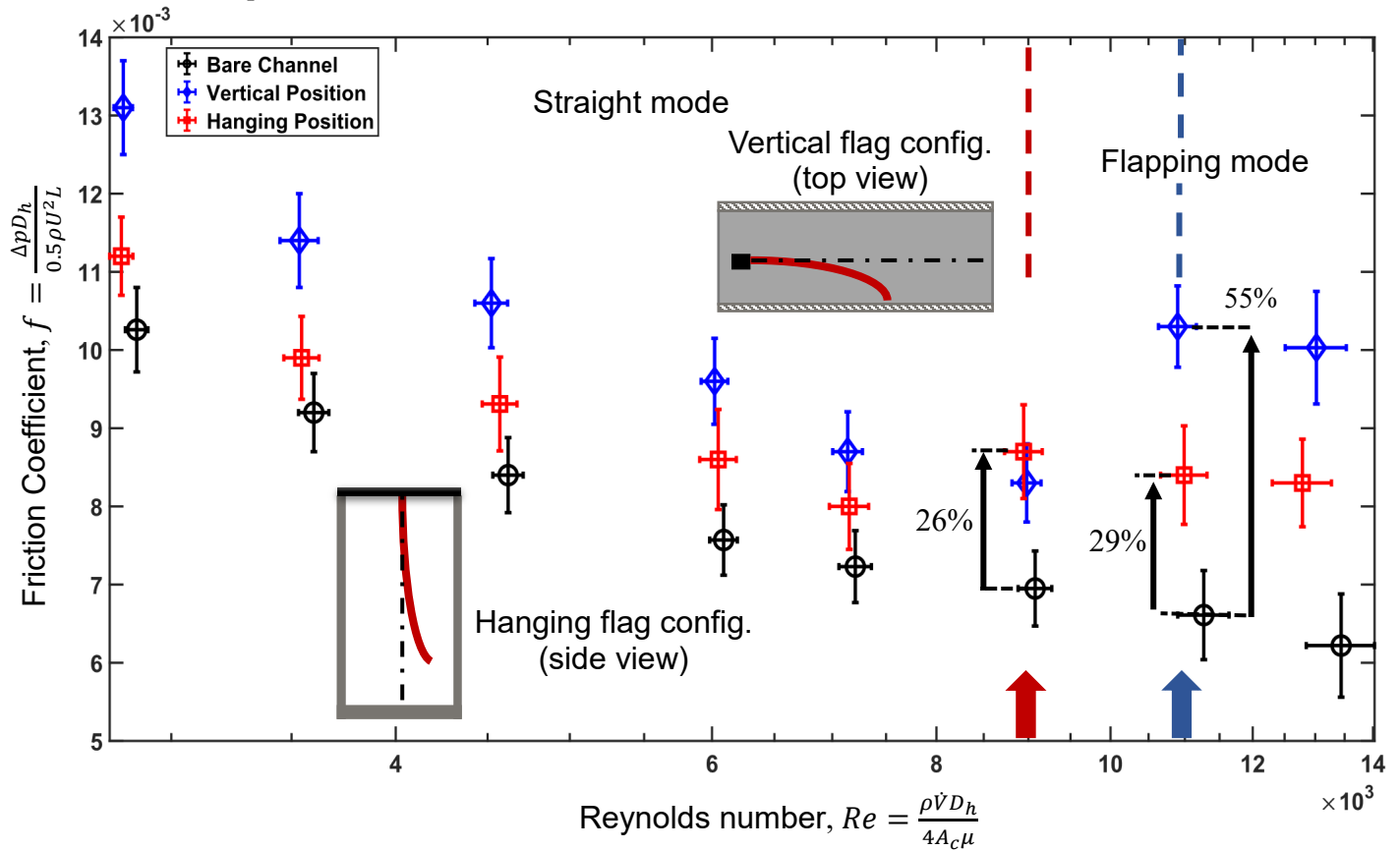


Fig. 4: The friction coefficient as a function of Re number. The transition to the flapping mode for the hanging and vertical configurations is shown by the red and blue arrow, respectively. In addition, the straight and flapping modes, for each flap configuration, are demarcated by the corresponding colored dashed lines. One rectangular flap was placed in the middle of each channel with a width, height, and length of 8.8 mm, 26 mm, and 300 mm, respectively. The inlet air temperature was fixed at 22.5 °C and the input power to the heater was set at 120 W. The transition to the fluttering mode for the vertical flap occurred at $Re = 11,270$ while the onset of the flapping for the hanging configuration occurred earlier at $Re = 8,940$.

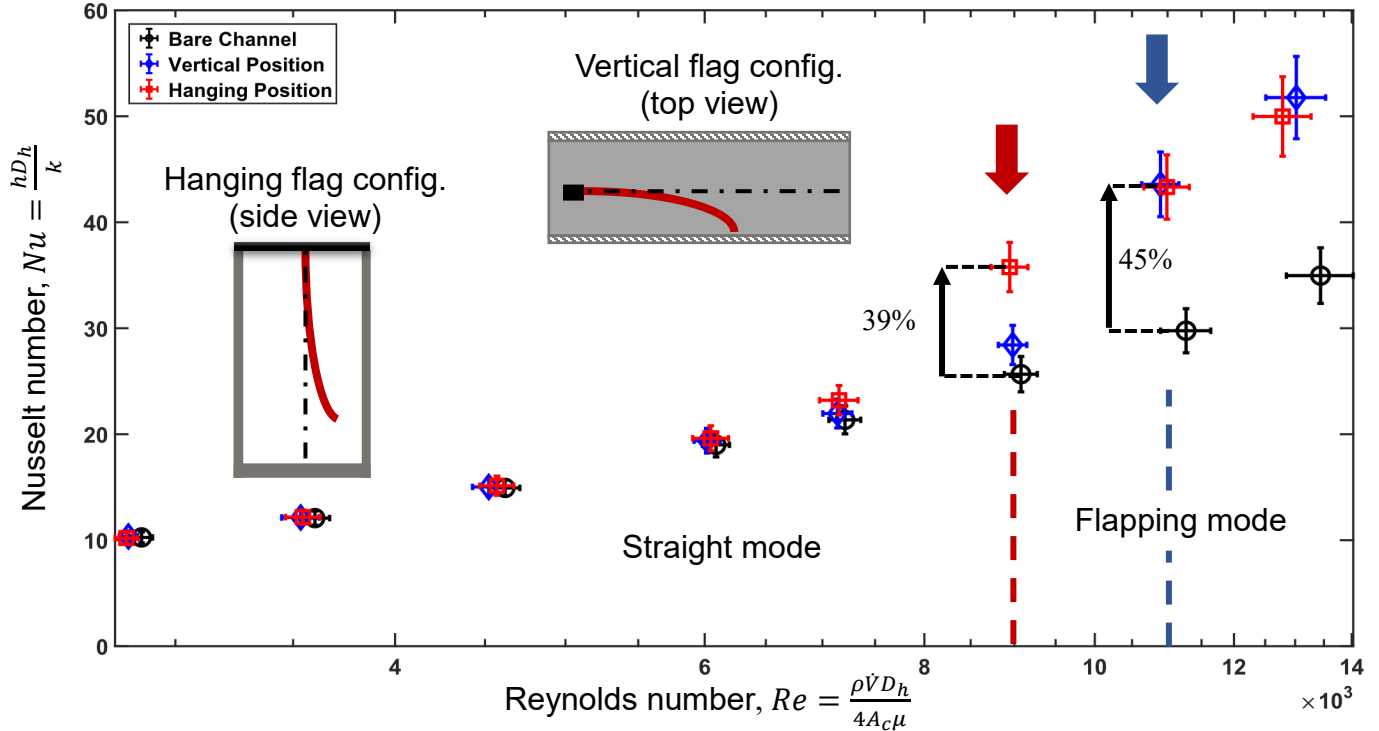


Fig. 5: The average Nu number with the increase in Re number. The transition to the flapping mode for the hanging and vertical configurations is shown by a red and blue arrow, respectively. In addition, the straight and flapping modes are demarcated for each flap configuration, by corresponding colored dashed lines. One rectangular flap was placed in the middle of each channel with a width, height, and length of 8.8 mm, 26 mm, and 300 mm, respectively. The inlet air temperature was set at 22.5 °C and the input power to the heater was fixed at 120 W. The transition to the fluttering mode in vertical flaps occurs at $Re = 11,270$ while the onset of flapping in the hanging configuration occurred earlier at $Re = 8,940$.

In terms of hydraulic performance, the hanging configuration showed a lower pressure drop compared to the vertical one in both the stretched and flapping modes, as can be seen in Fig. 3 and 4. In the stretched mode, the standard vertical flaps created an almost 20% more pressure drop increase compared to the bare channel, while the hanging flaps exerted a 13% pressure drop increase. This slightly higher pressure drop could be attributed to the presence of the flag mast. Similarly, in the flapping mode, the standard vertical flaps increased the friction coefficient by roughly 56%; this number was less than 34% for the hanging one. The reason for the higher hydraulic loss is the channel blockage at the end of each stroke of the flap. Conversely, the pressure drop which increases in the hanging configuration is mainly ascribed to the vibration of the flap itself, which mixes the flow and extracts energy from the flow to maintain its movement.

The Nu number of the channels equipped with the flaps compared to the bare channels is within the range of measurement uncertainty at a low Re value of $\leq 6,000$. However, the Nu number jumps at the outset of large amplitude oscillations due to the fluid-structure-interaction. The highest increase in the Nu number is nearly 45% for the hanging configuration. The vortices shed off the flaps interrupt the developing boundary layer leading to heat transfer enhancement. The generated vortices can penetrate the viscous boundary layer and agitate the flow.

Other performance metrics – the j-factor and thermal-hydraulic performance factor – are plotted against the Re number in Figs. 6 and 7, respectively.

As shown in Fig. 5, the Nu number increases monotonically with the Re number, however, the j-factor plot is a better representative for thermal performance that excludes the effect of the fluid momentum. The j-factor increased sharply by up to 50%, and the difference between the hanging and vertical configurations in the flapping region ($Re \geq 10,900$) was negligible. The overall thermal-hydraulic performance of the heatsink augmented with a hanging flap was increased by 30% at the inception of the flapping mode, $Re = 8,940$. This translates into gaining a 30% increase in the heat transfer rate with no additional fan power, when compared to the vertical flap arrangement.

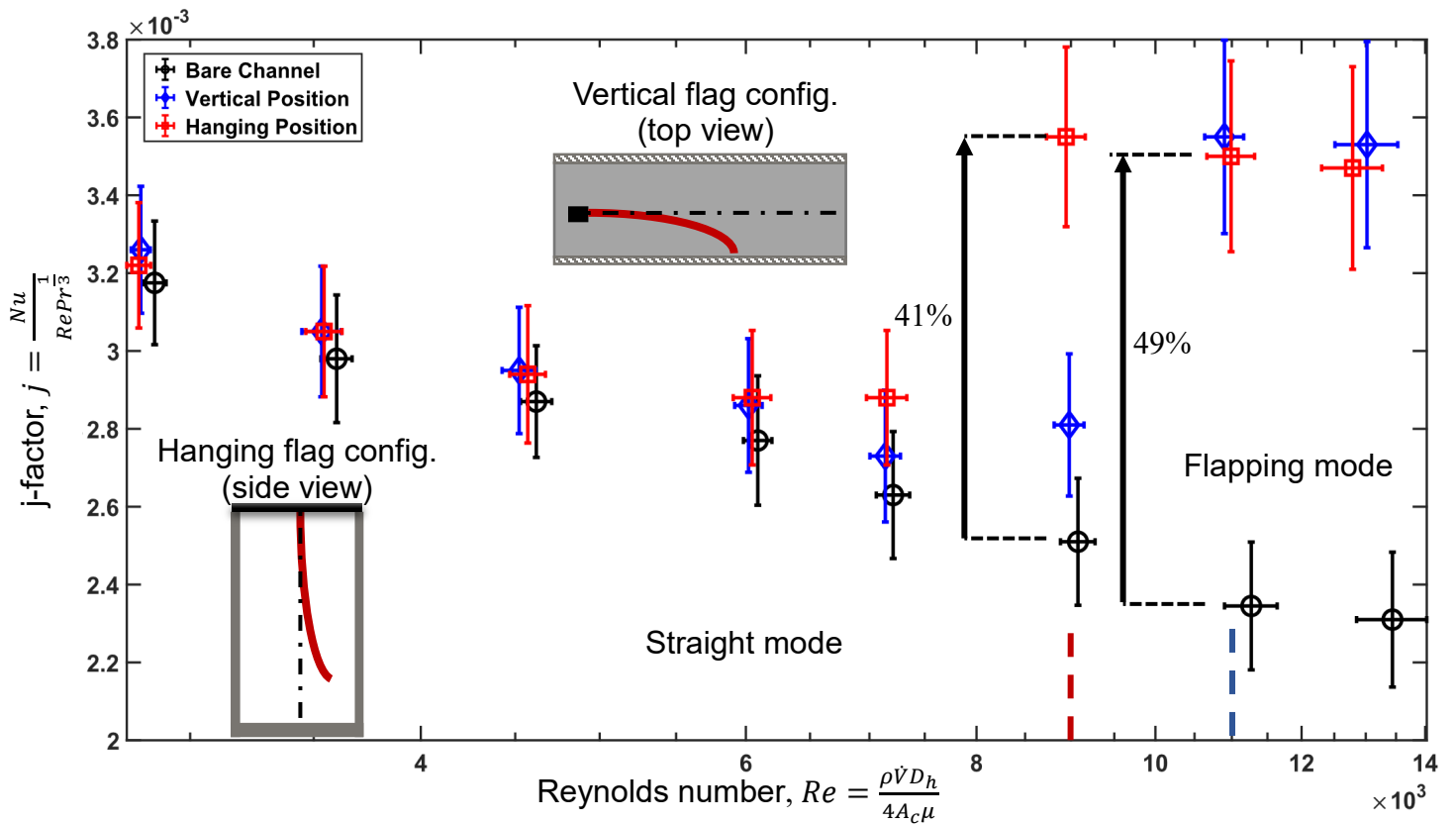


Fig. 6: The j-factor versus the Re number. The straight and flapping modes for the hanging/vertical configuration are demarcated by a red and blue dashed line, respectively. One rectangular flap was placed in the middle of each channel with a width, height, and length of 8.8 mm, 26 mm, and 300 mm, respectively. The inlet air temperature was set at 22.5 °C and the input power to the heater was fixed at 120 W. The transition to the fluttering mode in vertical flaps occurred at $Re = 11,270$ while the onset of the flapping mode in the hanging configuration occurred earlier at $Re = 8,940$.

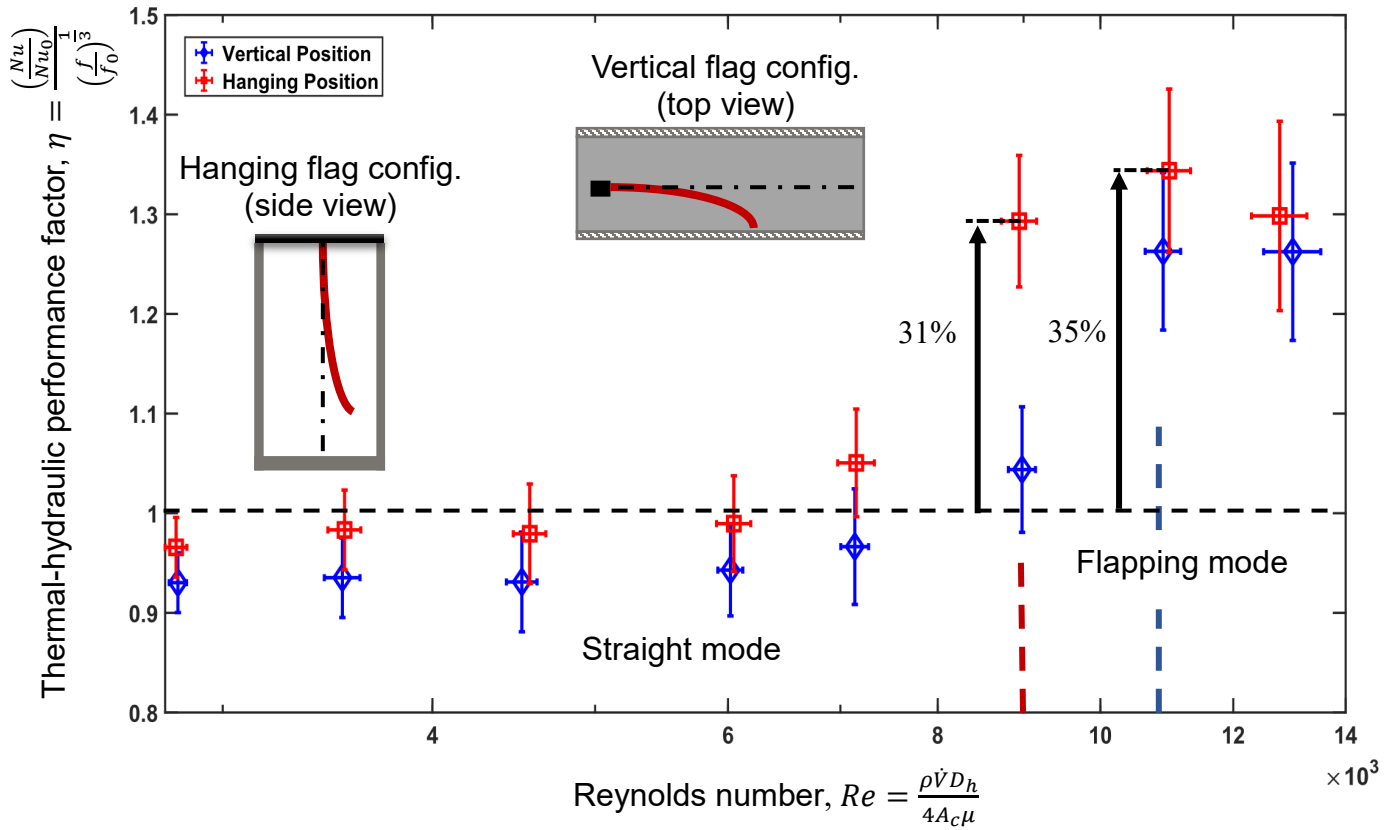


Fig. 7: The thermal-hydraulic performance factor for the two flap orientations. The inlet air temperature was set at 22.5 °C and the input power to the heater was fixed at 120 W. The straight and flapping modes for the hanging and vertical configuration are demarcated by a red and blue dashed line, respectively. One rectangular flap was placed in the middle of each channel with a width, height, and length of 8.8 mm, 26 mm, and 300 mm, respectively. The transition to the fluttering mode in the vertical flaps occurred at $Re = 11,270$ while the onset of flapping in hanging configuration occurred earlier at $Re = 8,940$.

4. Conclusions

In this study, an experimental investigation of nature-inspired fluttering flaps has been conducted in a wind tunnel in two positions: the hanging and vertical configuration. The downside of installing flaps vertically which is a higher critical flow velocity has been addressed in this paper by installing the flaps in the hanging configuration. It was observed that the boundary layer around the flap was shorter in the proposed hanging configuration, which made it more unstable, thus more effective. Other advantages of the hanging configuration over the vertical one was that there was less pressure drop increase due to the elimination of the channel blockage associated with the vertical installation of flaps. In addition, the need for a flag post was omitted, and the flaps were connected to the heatsink shroud directly. The lower hydraulic loss, critical flow velocity and the same heat dissipating performance made the hanging configuration a promising approach and a topic worthy of further investigation.

References

- [1] Z. Zhang, X. Wang, and Y. Yan, "A review of the state-of-the-art in electronic cooling," *e-Prime*, 2021, doi: 10.1016/j.prime.2021.100009.
- [2] Z. He, Y. Yan, and Z. Zhang, "Thermal management and temperature uniformity enhancement of electronic devices by micro heat sinks: A review," *Energy*, vol. 216, 2021, doi: 10.1016/j.energy.2020.119223.
- [3] J. M. Wu and W. Q. Tao, "Numerical study on laminar convection heat transfer in a rectangular channel with

- longitudinal vortex generator. Part A: Verification of field synergy principle,” *Int. J. Heat Mass Transf.*, vol. 51, no. 5–6, 2008, doi: 10.1016/j.ijheatmasstransfer.2007.03.032.
- [4] T. Alam, R. P. Saini, and J. S. Saini, “Use of turbulators for heat transfer augmentation in an air duct - A review,” *Renewable Energy*, vol. 62, 2014, doi: 10.1016/j.renene.2013.08.024.
- [5] C. Eloy, R. Lagrange, C. Souilliez, and L. Schouveiler, “Aeroelastic instability of cantilevered flexible plates in uniform flow,” *J. Fluid Mech.*, vol. 611, 2008, doi: 10.1017/S002211200800284X.
- [6] A. Kornecki, E. H. Dowell, and J. O’Brien, “On the aeroelastic instability of two-dimensional panels in uniform incompressible flow,” *J. Sound Vib.*, vol. 47, no. 2, 1976, doi: 10.1016/0022-460X(76)90715-X.
- [7] C. Q. Guo and M. P. Paidoussis, “Stability of rectangular plates with free side-edges in two-dimensional inviscid channel flow,” *J. Appl. Mech. Trans. ASME*, vol. 67, no. 1, 2000, doi: 10.1115/1.321143.
- [8] N. Yamaguchi, T. Sekiguchi, K. Yokota, and Y. Tsujimoto, “Flutter limits and behavior of a flexible thin sheet in high-speed flow- II: Experimental results and predicted behaviors for low mass ratios,” *J. Fluids Eng. Trans. ASME*, vol. 122, no. 1, 2000, doi: 10.1115/1.483228.
- [9] O. Doaré, D. Mano, and J. Carlos Bilbao Ludena, “Effect of spanwise confinement on flag flutter: Experimental measurements,” *Phys. Fluids*, vol. 23, no. 11, 2011, doi: 10.1063/1.3662127.
- [10] K. Li, S. Wang, Z. Ke, and C. L. Chen, “A novel caudal-fin-inspired hourglass-shaped self-agitator for air-side heat transfer enhancement in plate-fin heat exchanger,” *Energy Convers. Manag.*, vol. 187, 2019, doi: 10.1016/j.enconman.2019.03.048.
- [11] X. L. Zhong, S. Fu, K. C. Chan, L. Q. Wang, and C. Y. H. Chao, “Experimental and Numerical Study of Heat Transfer Performance of a Channel Flow with an Inverted Flag,” *SSRN Electron. J.*, 2022, doi: 10.2139/ssrn.4019290.
- [12] Y. Yu, Y. Liu, and X. Amandolese, “A Review on Fluid-Induced Flag Vibrations,” *Applied Mechanics Reviews*, vol. 71, no. 1, 2019, doi: 10.1115/1.4042446.
- [13] J. Zhang, S. Childress, A. Libchaber, and M. Shelley, “Flexible filaments in a flowing soap film as a model for one-dimensional flags in a two-dimensional wind,” *Nature*, vol. 408, no. 6814, 2000, doi: 10.1038/35048530.
- [14] L. Huang, “Flutter of cantilevered plates in axial flow,” *J. Fluids Struct.*, vol. 9, no. 2, 1995, doi: 10.1006/jfls.1995.1007.
- [15] N. Yamaguchi, K. Yokota, and Y. Tsujimoto, “Flutter limits and behaviors of a flexible thin sheet in high-speed flow-I: Analytical method for prediction of the sheet behavior,” *J. Fluids Eng. Trans. ASME*, vol. 122, no. 1, 2000, doi: 10.1115/1.483242.
- [16] M. Argentina and L. Mahadevan, “Fluid-flow-induced flutter of a flag,” *Proc. Natl. Acad. Sci. U. S. A.*, vol. 102, no. 6, 2005, doi: 10.1073/pnas.0408383102.
- [17] X. L. Zhong, S. C. Fu, K. C. Chan, G. Yang, H. H. Qiu, and C. Y. H. Chao, “Experimental study on the thermal-hydraulic performance of a fluttering split flag in a channel flow,” *Int. J. Heat Mass Transf.*, vol. 182, 2022, doi: 10.1016/j.ijheatmasstransfer.2021.121945.
- [18] Z. Li, X. Xu, K. Li, Y. Chen, Z. Ke, S. Wang, H. Chen, G. Huang, C. L. Chen, C. H. Chen, “Bio-inspired self-agitator for convective heat transfer enhancement,” *Appl. Phys. Lett.*, vol. 113, no. 11, 2018, doi: 10.1063/1.5046502.
- [19] A. J. Mahvi, T. Kunke, R. V. Crystal, and S. Garimella, “Enhanced power plant air-cooled condensers using auto-fluttering reeds,” *Appl. Therm. Eng.*, vol. 193, 2021, doi: 10.1016/j.applthermaleng.2021.116956.
- [20] F. Herrault, P. A. Hidalgo, C. H. Ji, A. Glezer, and M. G. Allen, “Cooling performance of micromachined self-oscillating reed actuators in heat transfer channels with integrated diagnostics,” 2012, doi: 10.1109/MEMSYS.2012.6170408.
- [21] Z. Li, X. Xu, K. Li, Y. Chen, G. Huang, C. L. Chen, C. H. Chen, “Airfoil-shaped self-agitator for convective heat transfer enhancement,” *Int. J. Therm. Sci.*, vol. 133, 2018, doi: 10.1016/j.ijthermalsci.2018.07.038.
- [22] L. Tang and M. P. Paidoussis, “On the instability and the post-critical behaviour of two-dimensional cantilevered flexible plates in axial flow,” *J. Sound Vib.*, vol. 305, no. 1–2, 2007, doi: 10.1016/j.jsv.2007.03.042.
- [23] Z. Li, X. Xu, K. Li, Y. Chen, G. Huang, C. L. Chen, C. H. Chen, “A flapping vortex generator for heat transfer enhancement in a rectangular airside fin,” *Int. J. Heat Mass Transf.*, vol. 118, 2018, doi: 10.1016/j.ijheatmasstransfer.2017.11.067.
- [24] S. Ali, C. Habchi, S. Menanteau, T. Lemenand, and J. L. Harion, “Heat transfer and mixing enhancement by free elastic flaps oscillation,” *Int. J. Heat Mass Transf.*, vol. 85, 2015, doi: 10.1016/j.ijheatmasstransfer.2015.01.122.
- [25] W. M. Kays and J. H. Whitelaw, “Convective Heat and Mass Transfer,” *J. Appl. Mech.*, vol. 34, no. 1, 1967, doi:

10.1115/1.3607663.

- [26] R. J. Moffat, "Describing the uncertainties in experimental results," *Exp. Therm. Fluid Sci.*, vol. 1, no. 1, 1988, doi: 10.1016/0894-1777(88)90043-X.
- [27] M. P. Paidoussis, *Fluid-Structure Interactions: Slender Structures and Axial Flow: Second Edition*. 2016. doi: 10.1016/C2011-0-08058-4.